Use of Two Reference Points in Hypervolume-Based Evolutionary Multiobjective Optimization Algorithms

Hisao Ishibuchi[1(✉)], Ryo Imada[2], Naoki Masuyama[2], and Yusuke Nojima[2]

[1] Shenzhen Key Laboratory of Computational Intelligence, Department of Computer Science and Engineering, Southern University of Science and Technology, Shenzhen 518055, China
hisao@sustc.edu.cn

[2] Department of Computer Science and Intelligent Systems, Graduate School of Engineering, Osaka Prefecture University, 1-1 Gakuen-cho, Naka-ku, Sakai, Osaka 599-8531, Japan
ryo.imada@ci.cs.osakafu-u.ac.jp, {masuyama,nojima}@cs.osakafu-u.ac.jp

Abstract. Recently it was reported that the location of a reference point has a dominant effect on the optimal distribution of solutions for hypervolume maximization when multiobjective problems have inverted triangular Pareto fronts. This implies that the use of an appropriate reference point is indispensable when hypervolume-based EMO (evolutionary multiobjective optimization) algorithms are applied to such a problem. However, its appropriate reference point specification is difficult since it depends on various factors such as the shape of the Pareto front (e.g., triangular, inverted triangular), its curvature property (e.g., linear, convex, concave), the population size, and the number of objectives. To avoid this difficulty, we propose an idea of using two reference points: one is the nadir point, and the other is a point far away from the Pareto front. In this paper, first we demonstrate that the effect of the reference point is strongly problem-dependent. Next we propose an idea of using two reference points and its simple implementation. Then we examine the effectiveness of the proposed idea by comparing two hypervolume-based EMO algorithms: one with a single reference point and the other with two reference points.

Keywords: Evolutionary multiobjective optimization (EMO) · Hypervolume-based algorithms · Reference point specification · Hypervolume contribution

1 Introduction

The hypervolume indicator [25] has been used for performance comparison in the EMO (evolutionary multiobjective optimization) community [26] due to its Pareto compliant property [24]. The hypervolume indicator has also been used in indicator-based EMO algorithms such as SMS-EMOA [3, 8], HypE [2], and FV-MOEA [18]. In

A. Auger et al. (Eds.): PPSN 2018, LNCS 11101, pp. 384–396, 2018.
https://doi.org/10.1007/978-3-319-99253-2_31

this paper, these algorithms are referred to as the hypervolume-based EMO algorithms. Their high performance on many-objective problems has been reported in the literature [10, 21, 22] in comparison with Pareto dominance-based EMO algorithms (e.g., NSGA-II [6]). Whereas the Pareto dominance-based selection pressure towards the Pareto front is severely weakened by the increase in the number of objectives, the hypervolume indicator can drive the population towards the Pareto front (usually at the cost of large computation load for many-objective problems [10]).

Properties of the hypervolume indicator can be visually examined by using the optimal distribution of solutions for hypervolume maximization. The optimal distribution has been theoretically derived for two-objective problems [1, 4] and empirically shown for multiobjective problems with three or more objectives [12–14]. Let us consider a two-objective minimization problem whose Pareto front is a straight line between (0, 1) and (1, 0) in a two-dimensional objective space. In Fig. 1, the Pareto front is shown by the red line. The optimal distribution of μ solutions for hypervolume maximization is the equidistant distribution including (0, 1) and (1, 0) if the reference point $\boldsymbol{r}$ = (r, r) for hypervolume calculation satisfies $r \geq 1 + 1/(\mu - 1)$ [1, 4]. This condition is $r \geq 1.25$ in Fig. 1 with $\mu = 5$. Thus the optimal distribution includes the two extreme points (0, 1) and (1, 0) of the Pareto front when $r \geq 1.25$ as shown in Fig. 1(c) and (d). When $r < 1.25$, these two points are not included in the optimal distribution as shown in Fig. 1(a) and (b). It should be noted that the location of the reference point has no effect on the optimal distribution of solutions in Fig. 1 when $r \geq 1.25$. This observation suggests the use of a reference point which is far away from the Pareto front. Actually, the use of an infinitely large (i.e., distant) reference point in SMS-EMOA was mentioned in [8]. The reference point in SMS-EMOA in [3] was specified by adding 1.0 to the estimated nadir point in each generation (i.e., 2.0 in Fig. 1 if the true nadir point is correctly estimated).

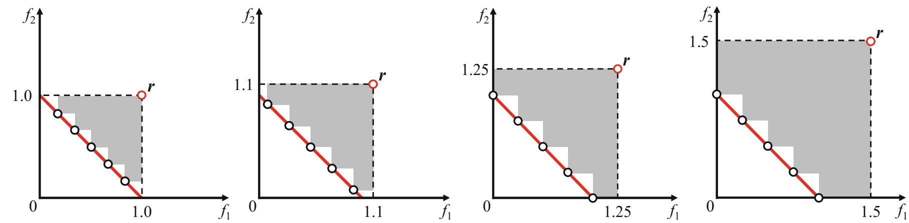

(a) r = 1.0 (nadir point). (b) r = 1.1. (c) r = 1.25. (d) r = 1.5.

Fig. 1. The optimal distribution of five solutions (μ = 5) for each specification of the reference point r = (r, r). The shaded area shows the corresponding hypervolume. (Color figure online)

The above discussions imply that the reference point specification is not important in the hypervolume-based EMO algorithms. When the reference point is far away from the Pareto front of the two-objective minimization problem as in Fig. 1(d), the hypervolume-based EMO algorithms work well. In this case, the two extreme points (0, 1) and (1, 0) have much larger hypervolume contributions than the other three inside solutions. As a result, the two extreme points of the Pareto front are likely to be found. When the two extreme points are included in the current population, the location of the reference point has no effect on the hypervolume contributions of the other inside solutions. For example, the three inside solutions have the same hypervolume contributions in Fig. 1(c) with $r = 1.25$ and Fig. 1(d) with $r = 1.5$.

A large reference point (which is far away from the Pareto front) can also be used for multiobjective minimization problems with triangular Pareto fronts such as the DTLZ1-4 [7] and WFG4-9 [9]. For example, in the case of three objectives, the hypervolume contributions of only the three extreme points of the Pareto front depend on the location of the reference point when they are included in the current population. Figure 2 shows approximately optimal distributions of 50 solutions of the three-objective DTLZ1 for two settings of the reference point $\boldsymbol{r} = (r, r, r)$: $r = 0.5$ (i.e., nadir point) in Fig. 2(a) and $r = 20$ in Fig. 2(b). These two distributions were obtained by SMS-EMOA with a large computation load (i.e., 1,000,000 generations) in our former study [12]. In Fig. 2(a) with $r = 0.5$, the three extreme points are not included in the obtained distribution since the nadir point is used as the reference point (i.e., since the hypervolume contributions of the three extreme points are zero when the nadir point is used as the reference point). In Fig. 2(b) with $r = 20$, the entire Pareto front is covered by the 50 solutions. Moreover, the two distributions in Fig. 2 are similar to each other whereas the totally different reference points are used. Figure 2 suggests that the use of a large reference point (which is far away from the Pareto front) works well on the three-objective DTLZ1. Figure 2 also suggests that the reference point specification is not important (since the similar results are obtained from the totally different reference points). Similar results are also obtained from the totally different reference points for the three-objective DTLZ2-4 and WFG4-9. It should be noted that the information of the true nadir point is used in those computational experiments (e.g., Fig. 2) to search for the optimal distribution of solutions.

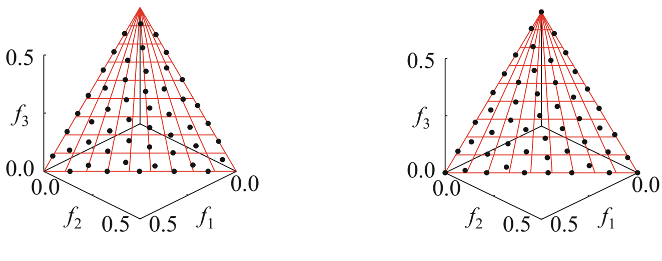

(a) $r = 0.5$ (nadir point). (b) $r = 20$.

Fig. 2. An approximately optimal distribution of 50 solutions ($\mu = 50$) of the three-objective DTLZ1 test problem for each specification of the reference point $r = (r, r, r)$ [12].

Our discussions on Figs. 1 and 2 suggest the use of a large reference point in the hypervolume-based EMO algorithms. This is a good idea for two-objective minimization problems and multiobjective minimization problems with triangular Pareto fronts. However, this is not a good idea for multiobjective minimization problems with

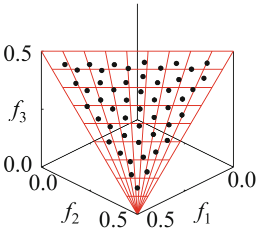

(a) $r = 0.5$ (nadir point).

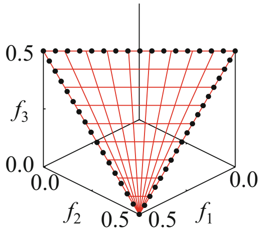

(b) $r = 20$.

Fig. 3. An approximately optimal distribution of 50 solutions ($\mu = 50$) of the three-objective inverted DTLZ1 test problem for each specification of the reference point $r = (r, r, r)$ [12].

inverted triangular Pareto fronts such as the inverted DTLZ1 [17], Minus-DTLZ1-4 [16] and Minus-WFG4-9 [16]. Figure 3 shows approximately optimal distributions of 50 solutions of the three-objective inverted DTLZ1 for the two settings of the reference point: $r = 0.5$ (i.e., nadir point) in Fig. 3(a) and $r = 20$ in Fig. 3(b). These two distributions were obtained by SMS-EMOA after 1,000,000 generations in our former study [12]. Figure 3(b) clearly shows that the use of a large reference point is not appropriate in the hypervolume-based EMO algorithms. The use of the nadir point is not appropriate as shown in Fig. 3(a), either.

An appropriate specification of the reference point was discussed from a viewpoint of fair performance comparison of EMO algorithms in our former studies [13, 14]. The basic idea is to specify the reference point so that uniformly distributed solutions over the entire Pareto front have similar hypervolume contributions (i.e., any solution should not have a dominantly large or negligibly small contribution). For the two-objective minimization problem with the linear Pareto front in Fig. 1, the suggested reference point in [13, 14] is $r = 1 + 1/(\mu - 1)$ where μ is the population size. In Fig. 1 with the population size 5, r is calculated as $r = 1.25$. This specification is used in Fig. 1(c) where each solution has exactly the same hypervolume contribution. By using an integer parameter H which denotes the number of intervals determined by μ solutions (i.e., $H = \mu - 1$), the suggested specification is rewritten as $r = 1 + 1/H$. The integer parameter H in this formulation is the same as H in the weight vector specification mechanism in MOEA/D [23]. Using this fact, the reference point specification method by $r = 1 + 1/H$ was extended to multiobjective minimization problems with linear Pareto fronts in [13, 14] where the value of H was determined from the number of objectives M and the population size μ using the following formulation:

$$ {}_{H+M-1}C_{M-1} \leq \mu < {}_{H+M}C_{M-1}. \tag{1} $$

In this formulation, ${}_nC_m$ denotes the number of combinations of selecting m elements from a set of n elements ($n \geq m$): ${}_nC_m = n!/m!(n - m)!$.

The reference point specification method of $r = 1 + 1/H$ with (1) is a good guideline for performance comparison of EMO algorithms. However, it does not always work well in the hypervolume-based EMO algorithms as we will show later in this paper. It is difficult to appropriately specify the reference point in the hypervolume-based EMO algorithms especially for multiobjective problems with nonlinear inverted triangular Pareto fronts (e.g., Minus-DTLZ2-4 and Minus-WFG4-9 [16]). This is because the appropriate reference point specification depends on various factors such as the shape of the Pareto front and its curvature property in addition to the number of objectives (M) and the population size (μ) used in (1). This is also because the true Pareto front is unknown (i.e., because the reference point specification should be based on the estimation nadir point, which is not always accurate).

To avoid the difficulty in appropriately specifying the reference point, we propose an idea of using two reference points. One is the estimated nadir point and the other is far away from it. Our idea is motivated by a simple intuition from Fig. 3: A good solution set would be obtained by combining the two solution sets in Fig. 3.

This paper is organized as follows. First, we demonstrate the difficulty in appropriately specifying the reference point in Sect. 2. Experimental results are explained using the hypervolume contributions of uniformly distributed solutions. Next, we propose an idea of using two reference points and its simple implementation in Sect. 3. Then, we examine the effectiveness of our idea in Sect. 4. Our two-point approach is compared with the standard single-point approach. Finally, we conclude this paper in Sect. 5 where a number of future research directions are suggested.

2 Empirical Discussions on Reference Point Specification

In this section, we show experimental results by FV-MOEA [18] on the three-objective DTLZ1 [7], DTLZ2 [7], Minus-DTLZ1 [16], Minus-DTLZ2 [16] and the car-side impact problem [17]. FV-MOEA is a recently-proposed fast hypervolume-based EMO algorithm. We use FV-MOEA in the same specifications as SMS-EMOA. Thus the same experimental results are obtained from FV-MOEA and SMS-EMOA. We use FV-MOEA because it is faster than SMS-EMOA (whereas we used SMS-EMOA in our former studies [12–14]).

FV-MOEA is applied to each three-objective minimization problem. During its execution, the objective space is normalized using non-dominated solutions in each generation as follows (e.g., see [11]). First, non-dominated solutions in the current population are selected. Next, the minimum and maximum values of each objective are found in the selected non-dominated solutions. Then, each objective is normalized so that the minimum and maximum values are 0 and 1, respectively. FV-MOEA with various specifications of the reference point is used under the following settings.

Population size (μ): 100,
Termination condition: 100,000 solution evaluations,
Crossover: SBX (Crossover probability: 1.0, Distribution index: 20),
Mutation: PM (Mutation probability: 1/(String length), Distribution index: 20),
Number of runs: 11 runs.

Among the 11 runs for each specification of the reference point, a single run with the median hypervolume is selected and shown as the experimental result in this paper.

Since the population size is 100 for the three-objective problems (i.e., $\mu = 100$ and $M = 3$), the suggested reference point in [13, 14] is calculated from (1) as $r = 1 + 1/$

H = 13/12. In addition to this specification, we also examine the following values: r = 1.0 (the estimated nadir point), 1.05 (closer to the estimated nadir point than 13/12), 1.2 (slightly larger than 13/12), 1.5 (larger than 13/12) and 10 (far away from the Pareto front: much larger than the others). Experimental results are shown in Figs. 4, 5, 6, 7 and 8.

In Fig. 4 on DTLZ1 and Fig. 5 on DTLZ2, almost the same results are obtained when $r \geq 1.05$. These results suggest the use of a large reference point for multiobjective minimization problems with triangular Pareto fronts. These results also show that the reference point specification is not important for such a multiobjective problem as long as the reference point is not too close to the estimated nadir point.

However, in Figs. 6, 7 and 8, totally different results are obtained from different specifications of the reference point. When the reference point is far away from the estimated nadir point (i.e., r = 10), many solutions are around the boundary of the Pareto front. In this case, only a small number of solutions are obtained inside the Pareto front. Thus we can see from Figs. 6, 7 and 8 that a large reference point is not appropriate.

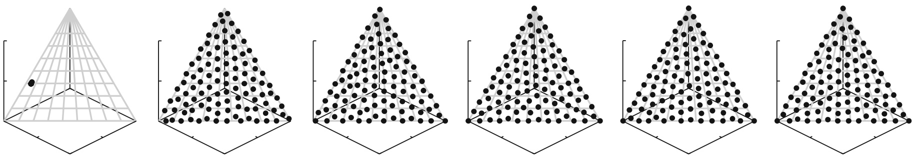

(a) r = 1.0. (b) r = 1.05. (c) r = 13/12. (d) r = 1.2. (e) r = 1.5. (f) r = 10.

Fig. 4. Experimental results on DTLZ1 (median results over 11 runs).

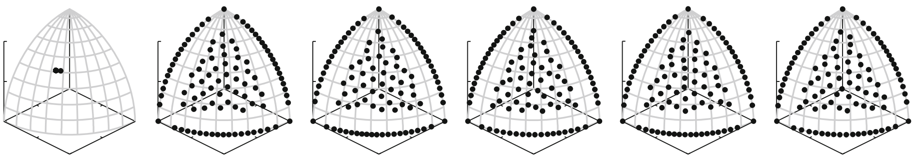

(a) r = 1.0. (b) r = 1.05. (c) r = 13/12. (d) r = 1.2. (e) r = 1.5. (f) r = 10.

Fig. 5. Experimental results on DTLZ2 (median results over 11 runs).

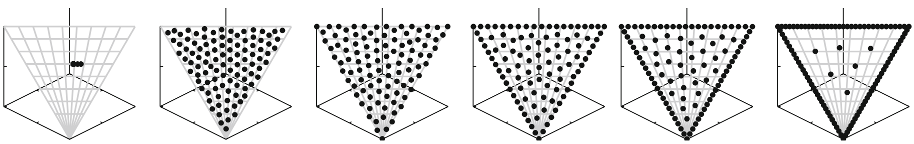

(a) r = 1.0. (b) r = 1.05. (c) r = 13/12. (d) r = 1.2. (e) r = 1.5. (f) r = 10.

Fig. 6. Experimental results on Minus-DTLZ1 (median results over 11 runs).

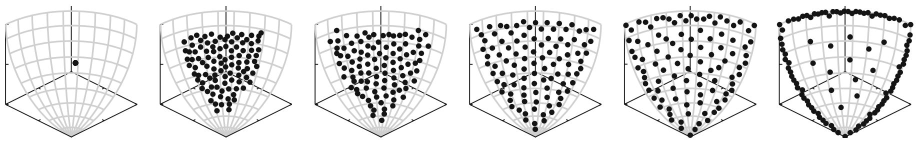

(a) $r = 1.0$. (b) $r = 1.05$. (c) $r = 13/12$. (d) $r = 1.2$. (e) $r = 1.5$. (f) $r = 10$.

Fig. 7. Experimental results on Minus-DTLZ2 (median results over 11 runs).

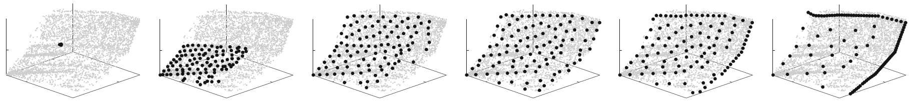

(a) $r = 1.0$. (b) $r = 1.05$. (c) $r = 13/12$. (d) $r = 1.2$. (e) $r = 1.5$. (f) $r = 20$.

Fig. 8. Experimental results on the car-side impact problem (median results over 11 runs).

Independent of the shape of the Pareto front, the use of the estimated nadir point (i.e., r = 1.0 in Figs. 4, 5, 6, 7 and 8(a)) is not advisable since the diversity of the obtained solution sets is very small. It should be noted that the obtained solution sets in Figs. 4(a) and 5(a) are totally different from the approximately optimal solution sets in Figs. 1(a) and 2(a), respectively. This is because the true nadir point is used in Figs. 1 and 2 while the estimated nadir point is used in Figs. 4, 5, 6, 7 and 8.

As shown in Figs. 4 and 5, for multiobjective problems with triangular Pareto fronts, the reference point specification is not important since almost the same solution sets are obtained from different specifications of the reference point as far as it is not too close to the estimated nadir point. On the contrary, for multiobjective problems with inverted triangular Pareto fronts, the reference point specification is important (see Figs. 6 and 7). However, it is difficult to appropriately specify the reference point for such a problem. For example, whereas the suggested reference point by $r = 1 + 1/H = 13/12$ works well on Minus-DTLZ1 in Fig. 6, it is too small for Minus-DTLZ2 in Fig. 7. In Fig. 7, r = 1.5 seems to be appropriate. However, it seems to be too large in Fig. 6 (compare Fig. 6(e) with Fig. 6(c) and (d)).

Our experimental results in Figs. 4, 5, 6, 7 and 8 can be explained using the hypervolume contributions of uniformly distributed solutions. In Figs. 9, 10, 11 and 12, we show the hypervolume contributions of 21 uniformly distributed solutions on the Pareto fronts. Each test problem in Figs. 9, 10, 11 and 12 is normalized so that the ideal and nadir points are (0, 0, 0) and (1, 1, 1), respectively. The 21 solutions are generated in the same manner as the weight vector generation mechanism in MOEA/D with H = 5. The suggested reference point by $r = 1 + 1/H$ is 1.2. In each figure, the size (i.e., area) of the closed circle is proportional to the hypervolume contribution of the corresponding solution. When the hypervolume contribution is zero, the corresponding solution is not shown.

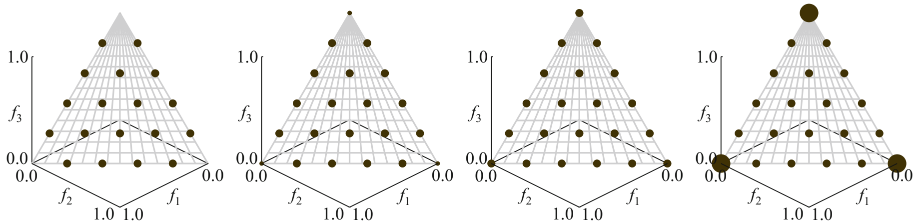

(a) $r = 1.0$. (b) $r = 1.1$. (c) $r = 1.2$. (d) $r = 1.5$.

Fig. 9. Hypervolume contribution of each solution of DTLZ1.

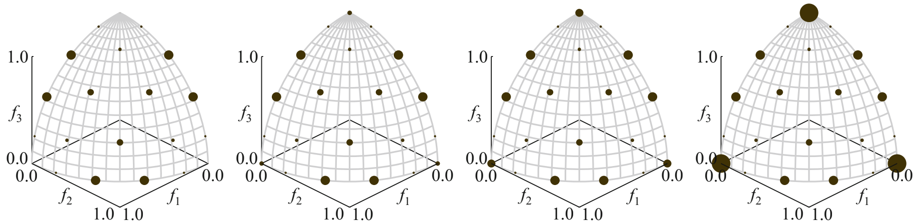

(a) $r = 1.0$. (b) $r = 1.1$. (c) $r = 1.2$. (d) $r = 1.5$.

Fig. 10. Hypervolume contribution of each solution of DTLZ2.

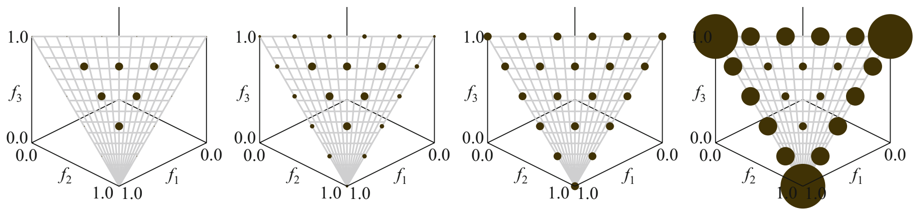

(a) $r = 1.0$. (b) $r = 1.1$. (c) $r = 1.2$. (d) $r = 1.5$.

Fig. 11. Hypervolume contribution of each solution of Minus-DTLZ1.

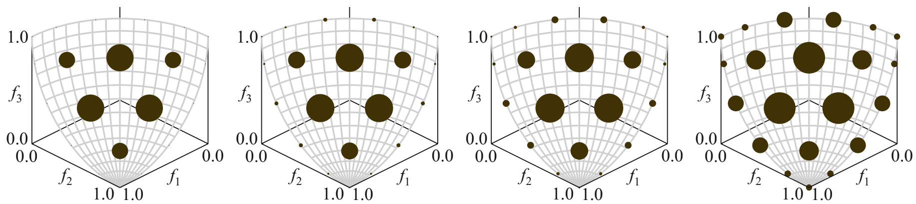

(a) $r = 1.0$. (b) $r = 1.1$. (c) $r = 1.2$. (d) $r = 1.5$.

Fig. 12. Hypervolume contribution of each solution of Minus-DTLZ2.

In Figs. 9, 10, 11 and 12(a) with $r = 1.0$, the hypervolume contributions of the three extreme points are zero. When the estimated nadir point is used as the reference point (i.e., $r = 1.0$) in the hypervolume-based EMO algorithms, the hypervolume contributions of the extreme points in the current population are zero. Thus they are likely to be removed from the current population through generation update. Then the diversity of the population gradually decreases, which increases the inaccuracy of the nadir point estimation. This is the reason for the very small diversity in Figs. 4, 5, 6, 7 and 8(a) with $r = 1.0$.

In Fig. 9 on DTLZ1 and Fig. 10 on DTLZ2, the hypervolume contributions of only the three extreme points depend on the reference point specification. This is the reason why almost the same results are obtained in Figs. 4 and 5 independent of the reference point specification except for the case where the reference point is too small. On the contrary, in Fig. 11 on Minus-DTLZ1 and Fig. 12 on Minus-DTLZ2, the reference point specification affects the hypervolume contributions of all boundary solutions. When the nadir point is used as the reference point in Figs. 11(a) and 12(a), the hypervolume contributions of all boundary solutions are zero. By increasing the distance between the reference point and the nadir point (i.e., by moving the reference point far away from the Pareto front), their hypervolume contributions increase. When the reference point is far away from the Pareto front, boundary solutions have large hypervolume contributions. This is the reason why only a small number of inside solutions are obtained in Figs. 6(f) and 7(f) with $r = 10$. The upper-right half of the Pareto front of the car-side impact problem in Fig. 8 has a similar property to the inverted triangular Pareto fronts of Minus-DTLZ1 and Minus-DTLZ2. Thus many solutions are obtained along the upper-right boundary of the Pareto front in Fig. 8(f).

When the suggested reference point (i.e., $r = 1.2$) is used for DTLZ1 in Fig. 9 and Minus-DTLZ1 in Fig. 11, all solutions in each figure have the same hypervolume contribution. This is the reason why the well-distributed solution sets are obtained for those test problems in Figs. 4(c) and 6(c). However, in Fig. 10 on DTLZ2 and Fig. 12 on Minus-DTLZ2, each solution has a different hypervolume contribution due to the nonlinearity of their Pareto fronts. As a result, well-distributed solution sets are not obtained in Figs. 5 and 7 independent of the reference point specification.

3 Proposed Idea and Its Simple Implementation

Our idea is to use two reference points in order to avoid the difficulty in appropriately specifying a single reference point for multiobjective problems with inverted triangular Pareto fronts. As the first attempt, we specify the two reference points as $r = 1.0$ and $r = 10$, respectively. That is, one reference point is the estimated nadir point, and the other is far away from it. The population is divided into two subpopulations of the same size. A hypervolume-based EMO algorithm (FV-MOEA [18] in this paper) is applied to each subpopulation using a different reference point: $r = 1.0$ for one subpopulation and $r = 10$ for the other. The final result of the proposed idea is the merged solution set of the two subpopulations. The execution of FV-MOEA is performed in each subpopulation separately except for the following two procedures.

(i) **Normalization:** The normalization of the objective space is performed in each generation using non-dominated solutions among all solutions in the two subpopulations. This is for accurately estimating the nadir point in each generation. If the normalization is performed separately, good results are not obtained from $r = 1.0$ as we have already shown in Figs. 4, 5, 6, 7 and 8(a) in the previous section.

(ii) **Periodical Subpopulation Comparison:** If the two subpopulations are similar, a good merged solution set cannot be obtained from them. In this case, it may be a good idea to merge them into a single population during the execution of FV-MOEA instead of merging them after its separate execution on each subpopulation. In this paper, we examine the similarity of the two subpopulations four times during its execution (after 20%, 40%, 60%, and 80% use of the available computation load, i.e., after 20,000th, 40,000th, 60,000th, and 80,000th solution evaluations). If the two subpopulations are similar, we merge them into a single population and FV-MOEA is applied to the merged population. The reference point is specified as $r = 1 + 1/H$. Once the two subpopulations are merged, the merged population is not divided again.

One important issue is how to measure the similarity of the two subpopulations. In this paper, we use the IGD$^+$ indicator [15] where the subpopulation with $r = 10$ is used as the IGD$^+$ reference points to calculate IGD$^+$ of the other subpopulation with $r = 1.0$. When the calculated IGD$^+$ is smaller than $2^{1/2}/5H$, we merge the two subpopulations. The threshold value is specified as $2^{1/2}/5H$ based on the following consideration. In the normalized three-objective DTLZ1, the length of each side of the triangular Pareto front is $2^{1/2}$ (e.g., the distance of the line between (1, 0, 0) and (0, 1, 0)). When $\mu = {}_{H+M-1}C_{M-1}$ solutions are uniformly distributed over the entire Pareto front, each side was divided into H intervals. Thus the distance between adjacent solutions on each side is $2^{1/2}/H$. The threshold value $2^{1/2}/5H$ is 1/5 of the distance between adjacent solutions on each side in the uniformly distributed solutions. Of course, other indicators (e.g., IGD [5, 20] and Δ_p [19]) and/or other specifications of the threshold value can be used, which is an important future research topic.

4 Experimental Results by the Proposed Idea

Using the same parameter specifications as in Sect. 2, we apply FV-MOEA with two reference points ($r = 1.0$ and $r = 10$) to the five test problems. Median experimental results among 11 runs are shown in Fig. 13.

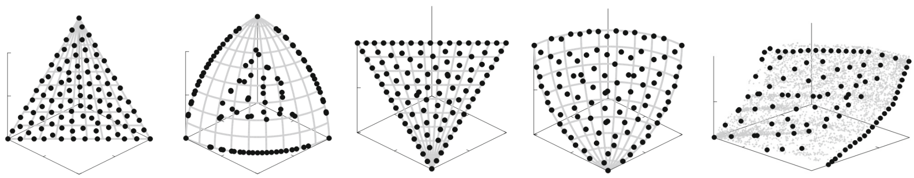

(a) DTLZ1. (b) DTLZ2. (c) Minus-DTLZ1. (d) Minus-DTLZ2. (e) Car-side.

Fig. 13. Experimental results by FV-MOEA with two reference points.

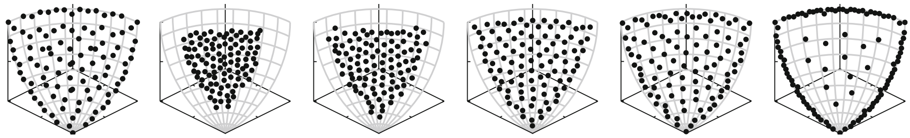

(a) $r = 1$ & 10. (b) $r = 1.05$. (c) $r = 13/12$. (d) $r = 1.2$. (e) $r = 1.5$. (f) $r = 10$.

Fig. 14. Comparison of the proposed idea with the standard single reference point approach.

In Fig. 13(c)–(d), we obtain the intended results. Many solutions around the boundary of the Pareto front of each test problem are obtained from $r = 10$. At the same time, many inside solutions are also obtained from $r = 1.0$. The effectiveness of the proposed idea is clearly shown in Fig. 13(d) for Minus-DTLZ2. In Fig. 14, we compare the obtained solution set by the proposed idea (i.e., Fig. 14(a) which is the same as Fig. 13(d)) with the results by the standard FV-MOEA with a single reference point (i.e., Fig. 14(b)–(f) which are the same as Fig. 7(b)–(f)). The solution set in Fig. 14(a) is similar to the solution set in Fig. 14(e) with $r = 1.5$. However, the boundary solutions in Fig. 14(a) are much closer to the boundary of the Pareto front than Fig. 14(e). That is, the solution set in Fig. 14(a) covers the wider region of the Pareto front than Fig. 14(e). Similar observations can be obtained from Fig. 13(c) and (e) by comparing them with the corresponding results of the standard FV-MOEA with a single reference point in Figs. 6 and 8, respectively.

The obtained solution set of DTLZ1 in Fig. 13(a) is almost the same as the solution sets in Fig. 4(c)–(f). This is because the two subpopulations are merged into a single population during the execution of FV-MOEA as intended. Once the two subpopulations are merged, FV-MOEA with the two reference points is exactly the same as FV-MOEA with $r = 1 + 1/H$. The obtained solution set of DTLZ2 in Fig. 13(b) seems to be inferior to the results in Fig. 5(b)–(f). This is because the two subpopulations are not merged in Fig. 13(b). By changing the threshold value from $2^{1/2}/5H$ to $2^{1/2}/2H$, almost the same solution set as Fig. 5(b)–(f) is obtained from FV-MOEA with the two reference points. This is because the two subpopulations are merged and FV-MOEA with $r = 1 + 1/H$ is used. This result suggests the necessity of further examinations about the parameter setting in the proposed idea.

5 Conclusions

In this paper, we proposed an idea of using two reference points in hypervolume-based EMO algorithms to avoid the difficulty in appropriately specifying a single reference point for multiobjective problems with inverted triangular Pareto fronts. Whereas promising results were obtained by a simple implementation of the proposed idea, a number of issues are left for future research to design a competent hypervolume-based EMO algorithm with two reference points. Among them are the choice of a similarity indicator and a threshold value, the timing of similarity check, and the specification of the two reference points (e.g., the use of an infinitely large reference point). Information exchange mechanisms between the two subpopulations should be further addressed.

Discussions are also needed on the estimation of the nadir point, the normalization of the objective space (e.g., see [11]), and the computational complexity of the proposed idea. Of course, performance comparison of the proposed idea with other EMO algorithms is needed. Another important future research topic is to examine the shape of the Pareto fronts of real-world multiobjective problems (e.g., triangular, inverted triangular or others; linear, concave or convex).

Acknowledgments. This work was supported by the Science and Technology Innovation Committee Foundation of Shenzhen (Grant No. ZDSYS201703031748284).

References

1. Auger, A., Bader, J., Brockhoff, D., Zitzler, E.: Hypervolume-based multiobjective optimization: theoretical foundations and practical implications. Theoret. Comput. Sci. **425**, 75–103 (2012)
2. Bader, J., Zitzler, E.: HypE: an algorithm for fast hypervolume-based many-objective optimization. Evol. Comput. **19**, 45–76 (2011)
3. Beume, N., Naujoks, B., Emmerich, M.: SMS-EMOA: multiobjective selection based on dominated hypervolume. Eur. J. Oper. Res. **181**, 1653–1669 (2007)
4. Brockhoff, D.: Optimal μ-distributions for the hypervolume indicator for problems with linear bi-objective fronts: exact and exhaustive results. In: Deb, K. (ed.) SEAL 2010. LNCS, vol. 6457, pp. 24–34. Springer, Heidelberg (2010). https://doi.org/10.1007/978-3-642-17298-4_2
5. Coello Coello, C.A., Reyes Sierra, M.: A study of the parallelization of a coevolutionary multi-objective evolutionary algorithm. In: Monroy, R., Arroyo-Figueroa, G., Sucar, L.E., Sossa, H. (eds.) MICAI 2004. LNCS (LNAI), vol. 2972, pp. 688–697. Springer, Heidelberg (2004). https://doi.org/10.1007/978-3-540-24694-7_71
6. Deb, K., Pratap, A., Agarwal, S., Meyarivan, T.: A fast and elitist multiobjective genetic algorithm: NSGA-II. IEEE Trans. Evol. Comput. **6**, 182–197 (2002)
7. Deb, K., Thiele, L., Laumanns, M., Zitzler, E.: Scalable multi-objective optimization test problems. In: Proceedings of IEEE CEC 2002, pp. 825–830 (2002)
8. Emmerich, M., Beume, N., Naujoks, B.: An EMO algorithm using the hypervolume measure as selection criterion. In: Coello Coello, C.A., Hernández Aguirre, A., Zitzler, E. (eds.) EMO 2005. LNCS, vol. 3410, pp. 62–76. Springer, Heidelberg (2005). https://doi.org/10.1007/978-3-540-31880-4_5
9. Huband, S., Hingston, P., Barone, L., While, L.: A review of multiobjective test problems and a scalable test problem toolkit. IEEE Trans. Evol. Comput. **10**, 477–506 (2006)
10. Ishibuchi, H., Akedo, N., Nojima, Y.: Behavior of multi-objective evolutionary algorithms on many-objective knapsack problems. IEEE Trans. Evol. Comput. **19**, 264–283 (2015)
11. Ishibuchi, H., Doi, K., Nojima, Y.: On the effect of normalization in MOEA/D for multi-objective and many-objective optimization. Complex Intell. Syst. **3**, 279–294 (2017)
12. Ishibuchi, H., Imada, R., Setoguchi, Y., Nojima, Y.: Hypervolume subset selection for triangular and inverted triangular Pareto fronts of three-objective problems. In: Proceedings of FOGA 2017, pp. 95–110 (2017)
13. Ishibuchi, H., Imada, R., Setoguchi, Y., Nojima, Y.: Reference point specification in hypervolume calculation for fair comparison and efficient search. In: Proceedings of GECCO 2017, pp. 585–592 (2017)

14. Ishibuchi, H., Imada, R., Setoguchi, Y., Nojima, Y.: How to Specify a Reference Point in Hypervolume Calculation for Fair Performance Comparison. Evolutionary Computation (in press)
15. Ishibuchi, H., Masuda, H., Tanigaki, Y., Nojima, Y.: Modified distance calculation in generational distance and inverted generational distance. In: Gaspar-Cunha, A., Henggeler Antunes, C., Coello, C.C. (eds.) EMO 2015. LNCS, vol. 9019, pp. 110–125. Springer, Cham (2015). https://doi.org/10.1007/978-3-319-15892-1_8
16. Ishibuchi, H., Setoguchi, Y., Masuda, H., Nojima, Y.: Performance of decomposition based many-objective algorithms strongly depends on Pareto front shapes. IEEE Trans. Evol. Comput. **21**, 169–190 (2017)
17. Jain, H., Deb, K.: An evolutionary many-objective optimization algorithm using reference-point based non-dominated sorting approach, part II: handling constraints and extending to an adaptive approach. IEEE Trans. Evol. Comput. **18**, 602–622 (2014)
18. Jiang, S., Zhang, J., Ong, Y.-S., Zhang, A.N., Tan, P.S.: A simple and fast hypervolume indicator-based multiobjective evolutionary algorithm. IEEE Trans. Cybern. **45**, 2202–2213 (2015)
19. Schütze, O., Esquivel, X., Lara, A., Coello Coello, C.A.: Using the averaged hausdorff distance as a performance measure in evolutionary multiobjective optimization. IEEE Trans. Evol. Comput. **16**, 504–522 (2012)
20. Sierra, M.R., Coello Coello, C.A.: A new multi-objective particle swarm optimizer with improved selection and diversity mechanisms. Technical report, CINVESTAV-IPN (2004)
21. Tanabe, R., Ishibuchi, H., Oyama, A.: Benchmarking multi- and many-objective evolutionary algorithms under two optimization scenarios. IEEE Access **5**, 19597–19619 (2017)
22. Wagner, T., Beume, N., Naujoks, B.: Pareto-, aggregation-, and indicator-based methods in many-objective optimization. In: Obayashi, S., Deb, K., Poloni, C., Hiroyasu, T., Murata, T. (eds.) EMO 2007. LNCS, vol. 4403, pp. 742–756. Springer, Heidelberg (2007). https://doi.org/10.1007/978-3-540-70928-2_56
23. Zhang, Q., Li, H.: MOEA/D: a multiobjective evolutionary algorithm based on decomposition. IEEE Trans. Evol. Comput. **11**, 712–731 (2007)
24. Zitzler, E., Brockhoff, D., Thiele, L.: The hypervolume indicator revisited: on the design of Pareto-compliant indicators via weighted integration. In: Obayashi, S., Deb, K., Poloni, C., Hiroyasu, T., Murata, T. (eds.) EMO 2007. LNCS, vol. 4403, pp. 862–876. Springer, Heidelberg (2007). https://doi.org/10.1007/978-3-540-70928-2_64
25. Zitzler, E., Thiele, L.: Multiobjective optimization using evolutionary algorithms—a comparative case study. In: Eiben, A.E., Bäck, T., Schoenauer, M., Schwefel, H.-P. (eds.) PPSN 1998. LNCS, vol. 1498, pp. 292–301. Springer, Heidelberg (1998). https://doi.org/10.1007/BFb0056872
26. Zitzler, E., Thiele, L., Laumanns, M., Fonseca, C.M., Fonseca, V.G.: Performance assessment of multiobjective optimizers: an analysis and review. IEEE Trans. Evol. Comput. **7**, 117–132 (2007)